# The representation of solar cycle signals in stratospheric ozone. Part II: Analysis of global models

Amanda C. Maycock[1], Katja Matthes[2,3], Susann Tegtmeier[2], Hauke Schmidt[4],
Rémi Thiéblemont[5], Lon Hood[6], Slimane Bekki[5], Makoto Deushi[7],
Patrick Jöckel[8], Oliver Kirner[9], Markus Kunze[10], Marion Marchand[11], Daniel
R. Marsh[12], Martine Michou[13], Laura E. Revell[14,15], Eugene Rozanov[14,16],
Andrea Stenke[14], Yousuke Yamashita[17,18], and Kohei Yoshida[7]

[1]School of Earth and Environment, University of Leeds, UK
[2]GEOMAR Helmholtz for Ocean Research, Kiel, Germany
[3]Christian-Albrechts Universität zu Kiel, Kiel, Germany
[4]Max Planck Institute for Meteorology, Hamburg, Germany
[5]LATMOS, Paris, France
[6]University of Arizona, Arizona, USA
[7]Meteorological Research Institute, Japan Meteorological Agency, Tsukuba, Japan
[8]Deutsches Zentrum für Luft- und Raumfahrt e.V. (DLR), Institut für Physik der Atmosphäre,
Oberpfaffenhofen, Germany
[9]Steinbuch Centre for Computing, Karlsruhe Institute of Technology, Karlsruhe, Germany
[10]Institut für Meteorologie, Freie Universität Berlin, Berlin, Germany
[11]Centre national de la recherche scientifique (CNRS), France
[12]National Center for Atmospheric Research, Boulder, USA
[13]CNRM UMR 3589, Météo-France/CNRS, Toulouse, France
[14]Institute for Atmospheric and Climate Science ETH, Zurich, Switzerland
[15]Bodeker Scientific, Christchurch, New Zealand
[16]Physikalisch-Meteorologisches Observatorium, World Radiation Center, Davos, Switzerland
[17]National Institute of Environmental Studies (NIES), Tsukuba, Japan
[18]now at: Japan Agency for Marine-Earth Science and Technology (JAMSTEC), Yokohama, Japan

*Correspondence to:* Amanda C. Maycock (a.c.maycock@leeds.ac.uk)

**Abstract.** The impact of changes in incoming solar irradiance on stratospheric ozone abundances should be included in climate model simulations to fully capture the atmospheric response to solar variability. This study presents the first systematic comparison of the solar-ozone response (SOR) during the 11 year solar cycle amongst different chemistry-climate models (CCMs) and ozone

5    databases specified in climate models that do not include chemistry. We analyse the SOR in eight CCMs from the WCRP/SPARC Chemistry-Climate Model Initiative (CCMI-1) and compare these with three ozone databases: the Bodeker Scientific database, the SPARC/AC&C database for CMIP5, and the SPARC/CCMI database for CMIP6. The results reveal substantial differences in the representation of the SOR between the CMIP5 and CMIP6 ozone databases. The peak amplitude of the

10    SOR in the upper stratosphere (1-5 hPa) decreases from 5% to 2% between the CMIP5 and CMIP6 databases. This difference is because the CMIP5 database was constructed from a regression model fit to satellite observations, whereas the CMIP6 database is constructed from CCM simulations,

which use a spectral solar irradiance (SSI) dataset with relatively weak UV forcing. The SOR in the CMIP6 ozone database is therefore implicitly more similar to the SOR in the CCMI-1 models than to the CMIP5 ozone database, which shows a greater resemblance in amplitude and structure to the SOR in the Bodeker database. The latitudinal structure of the annual mean SOR in the CMIP6 ozone database and CCMI-1 models is considerably smoother than in the CMIP5 database, which shows strong gradients in the SOR across the midlatitudes owing to the paucity of observations at high latitudes. The SORs in the CMIP6 ozone database and in the CCMI-1 models show a strong seasonal dependence, including large meridional gradients at mid to high latitudes during winter; such seasonal variations in the SOR are not included in the CMIP5 ozone database. Sensitivity experiments with a global atmospheric model without chemistry (ECHAM6.3) are performed to assess the impact of changes in the representation of the SOR and SSI forcing between CMIP5 and CMIP6. The experiments show that the smaller amplitude of the SOR in the CMIP6 ozone database compared to CMIP5 causes a decrease in the modelled tropical stratospheric temperature response over the solar cycle of up to 0.6 K, or around 50% of the total amplitude. The changes in the SOR explain most of the difference in the amplitude of the tropical stratospheric temperature response in the case with combined changes in SOR and SSI between CMIP5 and CMIP6. The results emphasise the importance of adequately representing the SOR in climate models to capture the impact of solar variability on the atmosphere. Since a number of limitations in the representation of the SOR in the CMIP5 ozone database have been identified, CMIP6 models without chemistry are encouraged to use the CMIP6 ozone database to capture the climate impacts of solar variability.

## 1 Introduction

Stratospheric heating rates are enhanced between the minimum and maximum phases of the approximately 11 year solar cycle through two main effects: absorption of enhanced incoming ultraviolet (UV) radiation and enhanced ozone concentrations (brought about by increased photochemical production) (e.g. Penner and Chang (1978); Brasseur and Simon (1981)). These radiative changes can drive feedbacks onto stratospheric dynamics, leading to amplified signals of solar cycle variability in regional surface climate via stratosphere-troposphere dynamical coupling (e.g. Kuroda and Kodera (2002)). To understand and model the impacts of solar cycle variability on the atmosphere and climate it is therefore necessary to account for the characteristics of spectral solar irradiance (SSI) variability and the associated solar-ozone response (SOR) (e.g. Haigh (1994)).

Maycock et al. (2016) examined the SOR in a number of recently updated satellite ozone datasets. This study focuses on the representation of the SOR in global climate and chemistry-climate models. At a minimum, models must include a sufficiently detailed representation of both SSI and the SOR to properly simulate solar cycle impacts on the atmosphere. The models routinely employed in Intergovernmental Panel on Climate Change (IPCC) and World Meteorological Organisation (WMO)

Ozone Assessment Reports typically represent atmospheric ozone in one of two ways. Chemistry-climate models (CCMs) include interactive stratospheric chemistry and explicitly simulate a SOR that is consistent with their photolysis, radiation and transport schemes provided that SSI variations are adequately (i.e. with sufficiently high spectral resolution) represented. A small, but growing, number of CCMs also include the chemical effects of galactic cosmic rays and solar energetic particles, though these effects are not explicitly considered in this study. Conversely, climate models do not routinely include interactive chemistry and must therefore prescribe a predefined ozone distribution to the radiation scheme taken from observations and/or models. Thus, if models without chemistry are to capture the full atmospheric response to solar variability, they must prescribe an ozone dataset that includes a representation of the SOR.

The World Climate Research Programme (WCRP) fifth Coupled Model Intercomparison Project (CMIP5) included models with and without interactive stratospheric chemistry. All CMIP5 models were recommended to prescribe SSI using the Naval Research Laboratory Spectral Solar Irradiance (NRLSSI-1) dataset (Wang et al., 2005); those without chemistry were further recommended to prescribe ozone from the Stratosphere-troposphere Processes And their Role in Climate (SPARC)/Atmospheric Chemistry and Climate (AC&C; www.igacproject.org) ozone database (Cionni et al. (2011); hereafter referred to as CMIP5 ozone database). The CMIP5 CCMs that fully resolved the stratosphere show a large variation in the amplitude and structure of the modelled SOR (Hood et al., 2015). This suggests that either the models implemented SSI differently, that there are large structural differences in the representation of chemical, dynamical or radiative processes between the models, and/or that the time series are too short to derive a robust SOR.

Differences in the representation of the SOR across CMIP5 models may have contributed to the large spread ($\sim$0.3-1.2 K) in the peak tropical stratospheric temperature response between solar minimum and maximum (Mitchell et al., 2015a). Other factors could include differences in the prescription of SSI and in the accuracy of the model radiation schemes (Nissen et al., 2007; Forster et al., 2011), but the quantitative importance of any one of these factors to explain the spread in modelled solar-climate responses is unclear. As was the case in CMIP5, CMIP6 will include a mixture of models with and without stratospheric chemistry. A new SPARC/CCMI ozone database has been created for CMIP6 models without chemistry (hereafter referred to as CMIP6 ozone database). It is therefore important to compare the SOR in the recommended CMIP5 and CMIP6 ozone databases, since any differences may lead to changes in the modelled responses to solar forcing between CMIP5 and CMIP6 models.

In addition to analysis of CMIP5 models (Hood et al., 2015), comparisons of the SOR in CCMs have been performed through the WCRP/SPARC Chemistry Climate Model Validation Exercises (CCMVal). The CCMVal-1 and CCMVal-2 models showed a positive annual mean SOR of up to $\sim$2.5% peaking in the tropics between $\sim$3-5 hPa and a maximum tropical mean temperature response in the upper stratosphere of $\sim$0.5-1.1 K (Austin et al., 2008; SPARC CCMVal, 2010). Vari-

85 ous developments have been made to models contributing to the latest SPARC Chemistry Climate Model Initiative (CCMI-1) experiments compared to previous versions, and it is therefore pertinent to evaluate the representation of the SOR in these new simulations.

Another potentially important factor to consider for modelling is the annual cycle in the SOR, which has been identified in available satellite observations (Maycock et al., 2016). Hood et al.

90 (2015) found that the three CMIP5 CCMs with the largest horizontal gradients in the fractional SOR in the upper stratosphere in early winter showed Northern hemisphere high latitude dynamical responses to the solar cycle that compared more closely with reanalysis data. The enhancement of the SOR at high latitudes is related to coupling between ozone and dynamics and may play a role in transferring the solar cycle signal from the upper stratosphere to the troposphere.

95 This study evaluates both the annual mean and annual cycle in the SOR in the CMIP5 and CMIP6 ozone databases and compares these with results from CCMI-1 models and satellite observations from Maycock et al. (2016). In addition to the CMIP ozone databases, we also analyse the recent Bodeker et al. (2013) ozone database for climate models (hereafter referred to as Bodeker ozone database). We further perform sensitivity experiments with a global atmospheric model to quantify

100 the impact of changes in the SOR between the CMIP5 and CMIP6 ozone databases on the atmospheric response between the minimum and maximum phases of the 11 year solar cycle. Collectively these analyses provide a comprehensive overview of the current representation of the SOR in global models and the importance of this representation for modelling the response to the solar cycle. The outline of the manuscript is as follows: Section 2 describes the data and methods used to analyse the

105 SOR, Section 3 presents the results, and Section 4 summarises our findings.

## 2 Methods

### 2.1 Models and ozone datasets

#### 2.1.1 The CCMI-1 models

Data are analysed from eight CCMI-1 models that were available from the British Atmospheric

110 Data Centre archive at the time the study was being prepared, and which include the minimum requirements for capturing the SOR (i.e. a prescription of SSI variability in the chemistry scheme). The models analysed are: CCSRNIES-MIROC3.2, CESM1(WACCM), CMAM, CNRM-CM5-3, EMAC(L90), LMDz-REPROBUS-CM5 (L39), MRI-ESM1r1, and SOCOL3 (see Table 1). A detailed description of the models is given by Morgenstern et al. (2017).

115 Data are analysed from the REF-C1 simulations, which include observed time-varying sea surface temperatures (SST) and sea ice from the Hadley Centre Sea Ice and Sea Surface Temperature (HadISST) dataset (Rayner et al., 2003), well-mixed greenhouse gases, volcanic aerosols, and the NRLSSI-1 SSI dataset that was also used in CMIP5 (Wang et al., 2005). CESM1(WACCM) uses

a merged SST dataset comprising of HadISST before 1981 and the NOAA Optimum Interpolation
120    dataset after 1981. Thus, in contrast to the coupled atmosphere-ocean CMIP5 models analysed by
Hood et al. (2015), the CCMI-1 REF-C1 simulations are run in AMIP mode and do not include an
interactive ocean. All the REF-C1 simulations start in January 1960, but terminate in different years
for each model, so for consistency we analyse the 50 year period 1960-2009, which is common to all
the simulations. We analyse one ensemble member (r1) for each model.

125    The representation of the QBO differs across the CCMI-1 models. Some of the models simulate a
spontaneous QBO (MRI-ESM1r1, EMAC(L90)), some models include a QBO by nudging tropical
stratospheric zonal winds towards observations (CCSRNIES-MIROC3.2, CESM1(WACCM), SO-
COL3), and some include no representation of the QBO (CMAM, CNRM-CM5-3, LMDz-REPROBUS-
CM5). In EMAC(L90) a weak nudging towards the observed QBO with a relaxation timescale of 58
130    days is applied to ensure the same phasing as the observed QBO, whereas in CCSRNIES-MIROC3.2,
CESM1(WACCM) and SOCOL3 the QBO is nudged more strongly (5-10 day timescale). For those
models that include QBO variability, two additional orthogonal QBO indices are included in the mul-
tiple linear regression (MLR) model which are calculated from the modelled tropical zonal winds
(see Section 2.2).

135    **2.1.2    The CMIP5 ozone database**

The CMIP5 ozone database consists of monthly mean ozone mixing ratios on 24 pressure levels
spanning 1000-1 hPa for the period 1850-2100. Data are provided on a regular 5/5° longitude/latitude
grid. Ozone values are provided as a 2-D (i.e. zonal mean) field in the stratosphere (at pressures less
than 300 hPa) and as a 3-D field in the troposphere, with a blending across the tropopause. The
140    tropospheric part of the database was constructed from CCM simulations. For the stratosphere, the
historical part of the database (1850-2009) was constructed from observations using an MLR model
(that includes solar variability as one of the independent variables) fit to SAGE I and SAGE II ver-
sion 6.2 satellite data and polar ozonesondes following Randel and Wu (2007). A SOR is therefore
implicitly included in the historical part of the CMIP5 ozone database that will resemble the in-
145    put observations fitted with the MLR model. However, owing to the paucity of long-term ozone
measurements at high latitudes, the SOR was only included between ±60° latitude. This limitation
led some CMIP5 modelling groups to make alterations to the CMIP5 ozone database, including
extrapolation of the SOR coefficients at ±50° latitude to the poles using a cosine latitude weight-
ing. The CMIP5 models known to have employed this 'Extended CMIP5 ozone database' include
150    HadGEM2-CC (Osprey et al., 2013), MPI-ESM (Schmidt et al., 2013) and CMCC-CC (Cagnazzo,
2016, pers. comms.). CMIP5 models with an upper boundary at pressures less than 1 hPa also had
to vertically extend the CMIP5 ozone database to include their upper boundary (e.g. Schmidt et al.
(2013); Osprey et al. (2013)).

The future part of the CMIP5 ozone database for the stratosphere was based on CCMVal-2 model
simulations (Cionni et al., 2011). However, owing to uncertainties in how individual CMIP5 models
would represent SSI variations over the 21st century, the future part of the CMIP5 ozone database
did not include a SOR. A SOR was then added to the future period in the Extended CMIP5 ozone
database using the solar MLR coefficients from the historical period (Schmidt et al. (2013); Osprey
et al. (2013); C. Cagnazzo, 2016, pers. comms.). Results are presented here from both the CMIP5
ozone database and the Extended CMIP5 ozone database for the period 1960-2004.

The CMIP5 ozone database is described in full by Cionni et al. (2011) and is available from:
http://cmip-pcmdi.llnl.gov/cmip5/forcing.html. Documentation of the CMIP5 models that employed
the CMIP5 ozone database is given by Eyring et al. (2013).

### 2.1.3 The CMIP6 ozone database

The CMIP6 ozone database for the historical period (1850-2014) consists of monthly mean ozone
mixing ratios on 66 pressure levels spanning 1000-0.0001 hPa. Data are provided as a 3-D field on
a regular $2.5 \times 1.9°$ longitude/latitude grid. The database has been constructed using output from
two CCMI-1 models (CESM1(WACCM) and CMAM), which have been weighted according to an
evaluation of various performance metrics for ozone (M. Hegglin, pers. comms.). The CCMs fol-
lowed the REF-C1 experiment protocol with prescribed observed SSTs, sea ice, well-mixed green-
house gas concentrations and aerosols. Observed estimates of surface emissions of $NO_x$ and other
tropospheric ozone precursor gases are prescribed. The two CCMs represent SSI in their radiation
and chemical schemes. Only CESM1(WACCM) includes the chemical effects of energetic particles,
which means the CMIP6 ozone database will only partly capture these effects. We analyse data from
the CMIP6 ozone database over the period 1960-2011. The CMIP6 ozone database was accessed
from: https://esgf-node.llnl.gov/projects/input4mips.

As is the case for all the CCMI-1 models, the two CCMs used to create the CMIP6 ozone database
were forced with the NRLSSI-1 dataset, whereas the CMIP6 models will be recommended to use
a new merged SSI dataset described by Matthes et al. (2017). The change in UV forcing between
solar cycle minimum and maximum is smaller in NRLSSI-1 than in the CMIP6 solar forcing dataset.
Specifically, the variability in the 200-400 nm band is around 30% smaller in NRLSSI-1 than in the
CMIP6 SSI dataset (Matthes et al., 2017). Sensitivity experiments with two CCMs reveal that the
weaker UV forcing in NRLSSI-1 reduces the amplitude of the tropical mean SOR in the stratosphere
by up ∼0.3% compared to a case forced with CMIP6 solar forcing (see Figure 7(c) in (Matthes et al.,
2017)). Therefore, there will be a small inconsistency between the amplitude of the SOR captured
in the CMIP6 ozone database and the SOR that would otherwise be simulated in a CCM forced with
the recommended CMIP6 solar forcing dataset.

### 2.1.4 The Bodeker ozone database

Bodeker et al. (2013) describe a new observationally based ozone database for climate models cov-
ering 1979-2007. Monthly and zonal mean ozone mixing ratios are provided on 70 pressure levels
spanning 878-0.05 hPa on a regular $5°$ latitude grid. The ozone field is constructed using a large num-
ber of satellite and ozonesonde observations from the Binary DataBase of Profiles (BDBP; Hassler
et al. (2008)) fitted with an MLR model including terms for equivalent effective stratospheric chlo-
rine (EESC), a linear trend, the QBO, the El Niño Southern Oscillation (ENSO), the solar cycle, and
the Mt Pinatubo volcanic eruption. We note that since the BDBP contains SAGE II v6.2 mixing ratio
data, this is likely to provide a strong constraint on the SOR in the tropics and subtropics because
SAGE II is a relatively long-term and stable ozone record. A single MLR fit is performed for all
points on a given pressure surface to enable regression coefficients to be derived for latitudes where
the observations are sparse (e.g. at high latitudes). We use the Tier 1.4 product from the Bodeker
ozone database, which is a spatially filled field that includes contributions from all the MLR basis
functions.

### 2.2 The multiple linear regression (MLR) model

The SOR is analysed using an MLR model as described by Maycock et al. (2016). Briefly, the zonal
mean ozone data are deseasonalised by removing the long-term monthly mean at each latitude and
pressure level. As in past studies, we then perform an MLR analysis on the timeseries of monthly
mean anomalies at each location, $O_3'(t)$, to diagnose the solar cycle component:

$$O_3'(t) = A \times F10.7(t) + B \times CO_2(t) + C \times EESC(t)$$
$$+ D \times ENSO(t) + E \times SAD_{volc}(t) + F \times QBO_A(t)$$
$$+ G \times QBO_B(t) + r(t), \qquad (1)$$

where $r(t)$ is a residual. The annual-mean SOR is calculated by regressing all months as a single
timeseries. The monthly SOR is calculated by regressing interannual timeseries of each month sepa-
rately. The monthly basis functions in Equation 1 are the F10.7cm radio solar flux, the $CO_2$ concen-
tration at Mauna Loa, the equivalent effective stratospheric chlorine (EESC), the Nino 3.4 index to
represent ENSO, and the volcanic aerosol surface area density ($SAD_{VOLC}$) averaged between $\pm30°$
latitude and 15-35 km. For those CCMI-1 models and ozone databases that include QBO variability
(see Table 1), the QBO indices are calculated as the first two principal component timeseries of the
tropical ($\pm10°$, 5-70 hPa) zonal mean zonal winds. Figure 1 shows example timeseries of the MLR
basis functions from 1960-2009 in arbitrary units. The coefficients A–G in Equation 1 are calculated
using linear least squares regression.

We use the F10.7cm flux to represent solar activity because it has been shown to be a better proxy
for UV radiation, the key driver of the stratospheric ozone response, than other indices, e.g. total solar
irradiance. The results presented in Section 3 assume a difference of 130 solar flux units (1 SFU =

$10^{-22}\,\mathrm{Wm^{-2}Hz^{-1}}$) as a representative amplitude of the 11 year solar cycle. The Nino 3.4 index is computed as the standardised mean SST averaged over the region 5°S–5°N and 120°W–170°W.

The only difference in the MLR model in Eqn. 1 compared to Maycock et al. (2016) is the addition of a basis function for stratospheric volcanic aerosol. This is because the analysis of longer timeseries, as performed here, reduces the issue of aliasing between the solar and volcanic timeseries (Chiodo et al., 2014). However, the inclusion of a volcanic basis function yields very similar results for the SOR to the method of excluding the periods immediately following large volcanic eruptions as was done by Maycock et al. (2016).

One important issue for MLR analysis is the handling of possible autocorrelation in the regression residuals, $r(t)$, and the effect on the estimation of statistical uncertainties. Some of the satellite ozone datasets considered by Maycock et al. (2016) had incomplete temporal sampling at a given location, which reduces the likelihood of significant autocorrelation in the residuals. However, by design the ozone fields analysed here have complete temporal sampling, and a Durbin-Watson test reveals significant serial correlation in the regression residuals in many locations for lags of one and two months, particularly in the lower stratosphere and mesosphere. Such serial correlation can lead to spurious overestimation of the statistical significance of the regression coefficients and we therefore include an autoregressive term in the regression model. Given the significant serial correlations in some regions up to a lag of two months, a second order autoregressive noise process (AR2) is used, which assumes the residuals $r(t)$ have the form:

$$r(t) = ar(t-1) + br(t-2) + w(t), \tag{2}$$

where $a$ and $b$ are constants and $w(t)$ is a white noise process. This is identical to the approach employed in Maycock et al. (2016) and the recent SPARC SI$^2$N analysis of ozone trends (Tummon et al., 2015; Harris et al., 2015). No autocorrelation term for the residuals is included in the analysis of the SOR annual cycle because the residuals for any given month are approximately uncorrelated from year-to-year.

### 2.3 Atmospheric model sensitivity experiments

To explore the atmospheric impacts of different representations of the SOR, simulations were carried out with the atmospheric general circulation model ECHAM6.3, which is an update of the ECHAM6.1 model (Stevens et al., 2013) used as atmospheric component of the Max Planck Institute Earth System Model (Giorgetta et al., 2013) in CMIP5 simulations. Model changes from version 6.1 to 6.3 are mainly related to fixes of bugs described by Stevens et al. (2013), efforts to ensure energy conservations, an update of the radiation scheme, which is now the PSrad (Pincus and Stevens, 2013) version of the RRTMG code (Iacono et al., 2008), and retuning. If the same forcings are used, temperature effects of solar cycle variability in ECHAM6.3 compare well to those described for ECHAM6.1 by Schmidt et al. (2013).

It is known that the ECHAM6.3 radiation code does not cover wavelengths below 200 nm and therefore the important Schumann-Runge bands and Lyman-alpha lines of ozone are not captured (Sukhodolov et al., 2014). This results in a too weak radiative response to the imposed solar forcing particularly in the mesosphere. Therefore we focus the analysis on the temperature response in the stratosphere where most of the absorption occurs at higher wavelengths and the performance is comparable to models with a more comprehensive radiative code (Sukhodolov et al., 2014).

We have performed five time-slice simulations with ECHAM6.3 each lasting for 50 years. The control simulation uses average boundary conditions as specified for the CMIP5 AMIP simulation, i.e. for all boundary conditions such as SSTs, greenhouse gas concentrations, solar irradiance and prescribed atmospheric ozone we have used multi-year averages of the CMIP5 recommended values for the years 1978 to 2008. Four sensitivity simulations have then been performed in which solar maximum minus solar minimum differences in either atmospheric ozone concentrations or both ozone and SSI have been added to the respective fields of the control simulation. For solar maximum and minimum conditions we have used average values over the years 1985-1986 and 1981-1982, respectively. According to the solar irradiance recommendations for CMIP6 (Matthes et al., 2017) these are characterized by a difference of 126.1 SFU, and are therefore closely comparable to the results presented for the SOR, which assume a representative solar cycle amplitude of 130 SFU. Ozone anomalies were either calculated from the respective years of the Extended CMIP5 ozone database (Schmidt et al. (2013)) or using the MLR regression coefficients for CMIP6 ozone database calculated below. Solar irradiance anomalies are either calculated from the CMIP5 recommended NRLSSI-1 dataset (Wang et al., 2005) or from the recommended CMIP6 solar forcing dataset (Matthes et al., 2017).

## 3   Results

### 3.1   The SOR in CCMI-1 models

Figure 2 shows timeseries of deseasonalised tropical (30°S-30°N) and monthly mean percent ozone anomalies at select pressure levels (1, 3, 5, 10, 30 hPa) for the eight CCMI-1 models considered in this study. The anomalies are defined relative to the period 1960-2009. These can be compared to Figures 2 and 8 in Maycock et al. (2016), which show equivalent timeseries for SAGE II and SBUV satellite ozone measurements.

The CCMI-1 models show a long-term decline in stratospheric ozone, particularly in the mid and upper stratosphere. This is consistent with the impact on ozone of increasing stratospheric inorganic chlorine and bromine abundances over this period (SPARC CCMVal (2010)). At 1 hPa, the trend in ozone between 1979-1997 computed by linear regression ranges from -1.9 to -2.6 % decade$^{-1}$ across the models. At 3 hPa, the range in trends is -4.1 to -5.1 % decade$^{-1}$. These values are within the uncertainty bounds of satellite observed ozone trends over this period (Harris et al., 2015).

In addition to a long-term decline in ozone, Figure 2 shows quasi-decadal variations in the upper stratosphere that are approximately in phase with the 11 year solar cycle; these are a marker of the SOR which is evident in the raw ozone timeseries before the MLR analysis is applied. There is larger interannual and multi-year variability in ozone at 10 and 30 hPa where some models show QBO signals.

Figure 3 shows latitude-pressure cross-sections of the annual mean SOR in the eight CCMI-1 models along with the multi-model mean (Figure 3(i)). All of the models show significant increases in ozone between solar minimum and maximum of around 1-2% between 1-10 hPa, which is less than half of the peak amplitude in the SAGE II v6.2 mixing ratio dataset, but is more comparable to the amplitude in SAGE II v7.0 mixing ratios and the SBUVMOD VN8.6 dataset (see Figures 4 and 12 in Maycock et al. (2016)).

The results in Figure 3 are broadly consistent with previous analyses of CCMs (Austin et al., 2008; SPARC CCMVal, 2010). The main exception to this is the absence in the multi-model mean of a significantly enhanced SOR in the tropical lower stratosphere. Figure 4(d) in Austin et al. (2008) shows a multi-model mean SOR for the CCMVal-1 models of around 5% per 130 SFU at ~50 hPa, as compared to around 1% in the CCMI-1 multi-model mean in Figure 3(i). However, there was large intermodel spread in this signal across the CCMVal-1 models and the multi-model mean SOR was dominated by strong responses in a few models that only ran for a short period (1980-2004) over which aliasing with the effects of volcanic aerosols can be significant (Chiodo et al., 2014). Since the CCMI-1 models are analysed for a longer period (1960-2009), this is a plausible explanation for the differences in tropical lower stratospheric SOR between the CCMI-1 and CCMVal-1 model responses.

Outside of the tropics there are larger inter-model differences in the fractional SORs in Figure 3, with a range in the amplitude, sign and level of statistical significance of the diagnosed SOR in both hemispheres. One consistent feature across many of the models appears to be an enhanced SOR in the Southern hemisphere high latitude lower stratosphere, which is evident in the multi-model mean. The annual cycles in the SOR in the individual models (see Supplementary Information) show that the strong gradients in the SOR at high latitudes found in some of the models tend to be more pronounced in the winter seasons. This behaviour, which is also seen in some satellite ozone datasets (Maycock et al., 2016), cannot be understood from photochemical processes alone and must therefore be related to stratospheric circulation changes (Kuroda and Kodera, 2002). Such changes in ozone at high latitudes will be associated with a radiative perturbation that could lead to feedbacks onto circulation; however, the quantitative importance of such ozone-radiative feedbacks for the stratospheric dynamical signal remains an open research question (Hood et al., 2015).

### 3.2 The SOR in ozone databases for climate models

325

Figure 4 shows timeseries from 1960-2012 of deseasonalised tropical and monthly mean fractional ozone anomalies at select stratospheric levels (1 to 30 hPa) from the Bodeker (orange line), CMIP5 (green) and CMIP6 (black) ozone databases. Anomalies are defined relative to the period 1979-2007. The Extended CMIP5 ozone database is not shown since this is identical to the green line. The plots

330     can be compared to Figure 2 and to Figures 2 and 8 in Maycock et al. (2016), which show equivalent timeseries for the SAGE II and SBUV satellite records.

Although the timeseries have been deseasonalised, the CMIP5 ozone database shows a residual annual cycle particularly in the upper stratosphere. This is the result of the annual cycle amplitude being larger in the early part of the record, when background ozone is relatively high, and smaller

335     in the later part of the record. Since the ozone anomalies in Figure 4 are plotted relative to 1979-2007, there is therefore a residual annual cycle in the CMIP5 ozone database particularly in the pre-1980 period. A similar effect is also evident in the Bodeker database, whereas the CMIP6 database, which is based on CCM simulations, does not show a significant change in the amplitude of the stratospheric ozone annual cycle over time.

340     At 1 hPa, the CMIP5 and Bodeker databases show a larger long-term trend in ozone diagnosed using linear regression over 1979-2007 of -3.5 % decade$^{-1}$ compared to a smaller trend of -1 % decade$^{-1}$ in the CMIP6 database; the latter being, as expected, similar to the long-term ozone trends in the CCMI-1 models shown in Figure 2. At 3 hPa, the CMIP5 ozone database shows a larger long-term trend by around a factor of two compared to the Bodeker and CMIP6 databases. Thus, the CMIP6

345     models that use the recommended CMIP6 ozone database might be expected to show a smaller cooling of the upper stratosphere over recent decades compared to an equivalent simulation using the CMIP5 database, owing to the smaller trend in ozone.

At 10 and 30 hPa, the Bodeker and CMIP6 databases show a QBO signal in ozone, whereas the CMIP5 database does not include QBO variability. This is an important distinction because a

350     model that employs the CMIP6 ozone database, but which does not simulate a dynamical QBO, will impose a QBO-ozone signal that may alter the model's behaviour. Alternatively, a model that internally generates a dynamical QBO that is not in phase with the QBO-ozone signal in the CMIP6 ozone database will be subject to a forcing by ozone that is inconsistent with the model's dynamical evolution. Both of these cases would be physically unrealistic. However, a model that nudges a QBO

355     towards observations and uses the CMIP6 ozone database should have a consistent representation of QBO variability in winds and ozone. Conversely, the absence of a QBO-ozone signal in the CMIP5 ozone database means that CMIP5 models that simulated a QBO would have neglected any radiative feedbacks from ozone onto tropical variability.

Figure 5 shows latitude-pressure cross-sections of the annual mean SOR in the three ozone databases

360     in Figure 4 and the Extended CMIP5 ozone database. In the tropics, the Bodeker ozone database, Figure 5(a), shows a positive SOR of up to 4% peaking at around 2-3 hPa with a distinct minimum

at ∼10 hPa. The latitudinal structure of the SOR is smoother than in the SAGE II v6.2 mixing ratio data (see Figure 4(d) of Maycock et al. (2016)) probably because the construction of the database uses MLR fitted to data along pressure surfaces rather than at individual latitudes. At high latitudes, the magnitude of the SOR in the Bodeker database is small and the spatial structure is noisy likely because of the small number of observations there. In the lower stratosphere, the results show a positive SOR at most latitudes, as was found in a number of satellite ozone datasets by Maycock et al. (2016).

The SOR in the CMIP5 ozone database, Figure 5(b), shows a very similar structure to that found in SAGE v6.2 mixing ratios (see Figure 4(d) of Maycock et al. (2016)), consistent with those data forming the backbone for the historical portion of the dataset (Cionni et al., 2011). Note that the MLR fitting was applied separately at each latitude band in the construction of the CMIP5 database, and this likely explains why the horizontal structure of the SOR is more heterogeneous than in the Bodeker ozone database. The sharp cut-offs in the SOR at ±60° latitude are spurious and result from a lack of data points to constrain the SOR at high latitudes. As described in Section 2.1.2, the Extended CMIP5 ozone database, Figure 5(c), applied a simple extrapolation to introduce a SOR in the extratropics. This structure, which shows a positive SOR in the northern extratropics and a negative SOR at pressures greater than ∼5 hPa polewards of 60°S, is likely to be subject to considerable uncertainties owing both to the large uncertainties in the observed SOR at these latitudes (Maycock et al., 2016) and the fact that the high latitudes are filled using a simple extrapolation method.

Figure 5(d) shows the SOR from the CMIP6 ozone database. The amplitude of the SOR is around 1-2% in the upper stratosphere consistent with the CCMI-1 results in Figure 3. This is 2-3 times smaller, and is considerably smoother in latitude, than the SOR in the CMIP5 ozone database. In the lowermost tropical stratosphere, the CMIP6 database shows a positive SOR of up to ∼3% in the southern tropics. The Bodeker database, Figure 5(a), also shows a strong positive SOR above the tropical tropopause although the structure is considerably less smooth in latitude. An enhanced SOR in the tropical lower stratosphere has been identified in satellite observations, albeit with large uncertainties (Gray et al., 2009; Austin et al., 2008; Soukharev and Hood, 2006; Maycock et al., 2016). It has been hypothesised that this feature may be dynamically forced by a weakening in the Brewer Dobson circulation between solar cycle minimum and maximum. However, some of the CCMI-1 models in Figure 3 do not show an enhanced SOR in the tropical lower stratosphere, suggesting this feature is not captured consistently amongst models and ozone datasets.

To further compare the structure of the SOR in the tropics, Figure 6 shows vertical profiles of the annual and tropical (30°S-30°N) mean SOR in the CCMI-1 models and climate model ozone databases. The range in the best estimate SOR across the CCMI-1 models is shown in dark grey shading, along with ±1 standard deviation of the intermodel spread. Observations from the SBU-VMOD VN8.6 (Frith et al., 2014) (black) and the SAGE-GOMOS 1 dataset (Kyrölä et al., 2015) (blue) are also shown (see Maycock et al. (2016) for details).

In the tropical lower stratosphere, the statistical uncertainties in the SOR are much larger than in
the rest of the profile, and the best estimate SOR ranges from a small negative signal in the CMIP5
ozone database to 6% in the Bodeker ozone database. The SOR in the CMIP6 database shows a
significant tropical mean SOR of 2% at 80 hPa, which is, as expected, within the range of the spread
in the CCMI-1 model signals. There is therefore a distinct difference in the representation of the
SOR in the tropical lower stratosphere in the CMIP5 and CMIP6 ozone databases, which may be
important for the modelled atmospheric response to solar variability in CMIP5 and CMIP6 models
(see Section 3.4). Figure 6 further confirms that the two climate model ozone databases that include
SAGE II v6.2 mixing ratio data (CMIP5 and Bodeker), show a substantially larger tropical mean
SOR in the upper stratosphere. This is consistent with Maycock et al. (2016) who concluded that the
SAGE II v6.2 mixing ratio data showed a considerably larger SOR in the tropical upper stratosphere
compared to SAVE II v7.0 mixing ratios and SBUV based datasets.

### 3.3 Comparison of SOR annual cycle in CMIP5 and CMIP6 ozone databases

Maycock et al. (2016) showed there are seasonal variations in the structure and amplitude of the
SOR estimated from satellite observations. Figure 7 shows the monthly mean SOR in the Extended
CMIP5 ozone database and Figure 8 shows the same for the CMIP6 ozone database. The SOR in
the CMIP5 database has a fixed structure and constant amplitude in all months; the small annual
cycle in the fractional SOR amplitude arises purely from the annual cycle in background ozone
concentrations. There are well understood photochemical arguments for why the structure of the
SOR is expected to track the position of the Sun through the year (Haigh, 1994). Furthermore,
the coupling between ozone and stratospheric dynamics may lead to variations in the SOR at high
latitudes in some months due to the formation in winter of the polar vortices and their subsequent
break-up in spring (Hood et al., 2015). For these reasons a complete absence of seasonal variation in
the SOR is unrealistic. In contrast, the SOR in the CMIP6 ozone database, Figure 8, shows greater
seasonal variation. Locally enhanced signals in the SOR are found in the southern high latitudes
and in the northern high latitudes in winter, which may be linked to variations in the strength of
the polar vortex (Kuroda and Kodera, 2002). Thus, the seasonal variability of the SOR in Figure
8 is likely to be more representative of the real atmosphere than the complete absence of seasonal
variability in Figure 7. However, there are quantitative differences between the SOR annual cycle in
the CMIP6 ozone database and that estimated from satellite observations (see Figure 13 of Maycock
et al. (2016)). These differences may result from uncertainties in estimating the SOR from relatively
short observational records, from errors in the representation of the SOR in the models used to
construct the CMIP6 ozone database, or a combination of factors. Thus there is a need for continued
satellite measurements in order to reduce the large uncertainties in the observed SOR, particularly
on seasonal timescales, and to provide a more stringent reference for ozone databases and models.

### 3.4 Atmospheric impact of change in SOR between CMIP5 and CMIP6 ozone databases

435 We now explore the atmospheric impacts of the differences between the SOR in the CMIP5 and CMIP6 ozone databases using the ECHAM6.3 model sensitivity experiments described in Section 2.3. Figure 9 shows the tropical average annual mean temperature differences in the four solar cycle perturbation simulations with respect to the control simulation. Note that the tropospheric temperature responses in all simulations are small because the model includes fixed SSTs and therefore the

440 troposphere does not fully adjust to the imposed solar forcing (e.g. Misios et al. (2016)).

The experiments performed to capture the total (i.e. SSI + SOR) solar cycle impact (dashed lines) show considerable differences in the tropical mean stratospheric temperature response between the recommended CMIP5 and CMIP6 forcings. In the CMIP5 case, the maximum temperature response is around 1.25 K near the stratopause, which can be compared to a much smaller response to the

445 CMIP6 solar forcing inputs of 0.7 K. The SOR-only sensitivity experiments (solid lines) reveal that much of the difference in the total temperature response can be attributed to the differences in the SOR between the CMIP5 and CMIP6 ozone databases. The SOR in the Extended CMIP5 ozone database induces a peak tropical temperature response of 0.9 K (solid red), which is three times larger than the maximum response to the SOR in the CMIP6 ozone database (solid blue). In addition

450 to the marked differences in the maximum temperature response, there are also distinct differences in vertical structure. In the CMIP5 case, there is a stronger vertical gradient in the temperature response, which can be attributed to the highly peaked structure of the SOR in the CMIP5 database at the stratopause compared to the smoother vertical structure of the SOR in the CMIP6 ozone database (cf. Figures 5(c) and 5(d)). The simulation forced with the SOR from the CMIP6 ozone database

455 also shows a small secondary peak in tropical lower stratospheric temperature of ∼0.3 K due to the presence of a locally enhanced SOR of ∼3%, which is not present in the CMIP5 ozone database. The results show that the change in the representation of the SOR between the recommended CMIP5 and CMIP6 ozone databases induces a much larger difference in the temperature response between solar cycle minimum and maximum than do changes in the recommended SSI forcing (see also Matthes

460 et al. (2017)).

The results from the ECHAM6.3 model help to elucidate the results of Mitchell et al. (2015a), which show a clear difference in the annual mean stratospheric temperature response to the solar cycle between CMIP5 models that used the CMIP5 ozone database (HadGEM2-CC, MPI-ESM, CMCC) and those with interactive chemistry that simulated their own internally-consistent SOR

465 (CESM1(WACCM), GFDL-CM3, GISS-E2-H, MIROC-ESM-CHEM, MRI-ESM1). Specifically, models that used the CMIP5 ozone database exhibit a markedly larger temperature response near the tropical stratopause, with a stronger vertical gradient, compared to the models with interactive chemistry. One might therefore anticipate that the difference in the stratospheric temperature response between solar cycle minimum and maximum for models with and without interactive chem-

470 istry will be smaller in CMIP6 than was found in CMIP5 owing to the fact that the SOR in the

CMIP6 ozone database is derived from CCM simulations, albeit forced with the CMIP5 SSI dataset that contains weaker UV variability than in the CMIP6 SSI dataset.

## 4    Conclusions

Changes in stratospheric ozone concentrations make a significant contribution to the atmospheric
475 response to changes in incoming solar radiation over the 11 year solar cycle (e.g. Shibata and Kodera (2005); Gray et al. (2009)). The associated solar-ozone response (SOR) must therefore be included in global model simulations to realistically represent solar influences on climate.

This study uses a multiple linear regression (MLR) model to analyse the SOR in eight chemistry-climate models (CCMs) from the CCMI-1 project: CCSRNIES-MIROC3.2, CESM1(WACCM),
480 CMAM, CNRM-CM5-3, EMAC(L90), LMDz-REPROBUS-CM5, MRI-ESM1r1, and SOCOL3. We also analyse the SOR in three ozone databases that are prescribed in climate models without in-teractive chemistry: the Bodeker et al. (2013) Tier 1.4 ozone database and the CMIP5 ozone database (Cionni et al., 2011), which are both based on regression models fit to observations, and the CMIP6 ozone database, which is created from historical simulations from two CCMs (CESM1(WACCM)
485 and CMAM).

The CCMI-1 models simulate a SOR with a peak amplitude of 1-2% in the upper stratosphere ($\sim$3-5 hPa). This is smaller than the SOR found in SAGE II v6.2 mixing ratio data and is more consistent with results from SAGE II v7.0 and SBUV satellite datasets (Maycock et al., 2016). Some of the CCMs show larger fractional SORs in the high latitude winter stratosphere, which are
490 strongly influenced by dynamical processes, although the amplitude and structure of these features tend to be less consistent across the models than the response in the tropical upper stratosphere. In addition, some of the models, in particular CMAM, LMDz-REPROBUS-CM5, MRI-ESM1r1 and SOCOL3, show an enhanced SOR in the tropical lower stratosphere, which has been identified in some satellite ozone datasets (Maycock et al., 2016). As expected, the SOR in the CMIP6 ozone
495 database generally resembles that in the CCMI-1 models, both in terms of its broad structure and magnitude and the fact that it includes seasonal variability. We note that since the UV variability in the SSI forcing dataset used in the CCMI-1 models is relatively weak, the SOR in the CMIP6 ozone database is smaller than would be simulated in a CCM forced with the CMIP6 SSI dataset, which includes larger UV variability (Matthes et al., 2017).

500 There are stark differences between the SOR in the CMIP6 ozone database and those found in the CMIP5 and Bodeker ozone databases. In particular, the peak amplitudes in the tropics are substan-tially larger (5%) in the latter databases compared to in the CMIP6 database (1.5%). This is because those databases are derived from observations that include SAGE II v6.2 mixing ratios, which as previously mentioned exhibit a larger SOR than found in other satellite ozone datasets (Maycock
505 et al., 2016).

In addition to differences in the peak magnitude of the SOR, there are also marked differences in the spatial structure of the SOR amongst the ozone databases. The CMIP5 database showed spurious large horizontal gradients in the SOR across the extratropics, which were reduced through implementation of a simple poleward extrapolation in the Extended CMIP5 ozone database (Schmidt et al.,
510   2013; Osprey et al., 2013). Furthermore, while the CMIP6 database implicitly includes seasonal variations in the SOR, as simulated by the CCMs used to construct the database, the CMIP5 database has a fixed annual mean SOR in all months, which is likely to be unrealistic. Given the inclusion of seasonal variations in the SOR compared to CMIP5, as well as the greater consistency with CCM results, CMIP6 models without chemistry are encouraged to use the recommended CMIP6 ozone
515   database (see esgf-node.llnl.gov/projects/input4mips). Nevertheless, whatever approach is adopted, all CMIP6 modelling groups are encouraged to document the representation of the SOR and SSI in their simulations to facilitate future analyses of solar-climate impacts.

Sensitivity experiments were performed using a comprehensive global atmospheric model without chemistry (ECHAM6.3) to test how the changes in the recommended SOR and SSI between
520   CMIP5 and CMIP6 affect the simulated annual mean temperature response over the 11 year solar cycle. The experiments show that changes in the SOR between CMIP5 and CMIP6 cause a decrease in the tropical average temperature response over the solar cycle of up to 0.6 K, or around 50%. This is the combined result of the SOR in the CMIP5 ozone database being very large due to it being based on SAGE II v6.2 mixing ratio data, and the SOR in the CMIP6 ozone database being some-
525   what weak because it is based on CCMs forced by the NRLSSI-1 dataset. The impact of changes in the recommended SOR on tropical stratospheric temperatures is many times larger than the separate impact (i.e. without ozone feedbacks) of changes in the recommended SSI forcing between CMIP5 and CMIP6. The results indicate that differences in the representation of the SOR amongst CMIP5 models is likely to be a major explanatory factor for the large spread in the stratospheric temperature
530   responses to the solar cycle in CMIP5 models (Mitchell et al., 2015a). The broader relevance of different representations of the SOR for atmospheric dynamics and regional surface climate responses to the solar cycle remains to be explored.

Substantial uncertainties remain in various factors related to understanding the SOR, which present challenges for including these effects in global models. Key issues include: outstanding large uncer-
535   tainties in the SOR derived from observations (Maycock et al., 2016); outstanding uncertainties in the characteristics of SSI variability (Ermolli et al., 2013; Haigh et al., 2010; Dhomse et al., 2016; Matthes et al., 2017); uncertainties in the ability of models to represent the effects of SSI variability on atmospheric radiation, photochemistry and dynamics (Forster et al., 2011; Sukhodolov et al., 2016; Hood et al., 2015; Matthes et al., 2017); and uncertainties in the magnitude of the observed
540   temperature response to the solar cycle (Ramaswamy et al, 2001; Mitchell et al., 2015b). Despite these various issues, information about the observed SOR has been used to exclude implausible scenarios for SSI variability (Ball et al., 2016) and this offers hope for further advances in understanding

the SOR in the future. Improved physical understanding and constraints for model performance rely on long-term high quality observational datasets and it is therefore vitally important that satellite

545 measurements of stratospheric ozone continue in the future.

*Acknowledgements.* ACM acknowledges funding from an AXA Postdoctoral Fellowship, the ERC ACCI Grant Project No. 267760, and a NERC Independent Research Fellowship (NE/M018199/1). ACM also acknowledges funding from the COST action ES1005 Towards a more complete assessment of the impact of solar variability on the Earth's climate (TOSCA) for a Short-term Scientific Mission to GEOMAR in September 2014 which

550 initiated this work. Parts of the work at GEOMAR Helmholtz Centre for Ocean Research Kiel was performed within the Helmholtz-University Young Investigators Group NATHAN, funded by the Helmholtz-Association and GEOMAR. The National Center for Atmospheric Research (NCAR) is sponsored by the U.S. National Science Foundation (NSF). WACCM is a component of the Community Earth System Model (CESM), which is supported by NSF and the Office of Science of the U.S. Department of Energy. The SOCOL team acknowledges

555 support from the Swiss National Science Foundation under grant agreement CRSII2_147659 (FUPSOL II). RT acknowledges his funding by the LABEX L-IPSL project (grant ANR-10-LABX-18-01). SB has been partially supported by the European project StratoClim (603557 under programme FP7-ENV.2013.6.1-2). We thank all of the CCMI-1 modelling groups who ran the simulations.

# References

560    Akiyoshi, H., Nakamura, T., Miyasaka, T., Shiotani, M., and Suzuki, M. A nudged chemistry-climate model simulation of chemical constituent distribution at northern high latitude stratosphere observed by SMILES and MLS during the 2009/2010 stratospheric sudden warming. *J. Geophys. Res.*, 121:1361–1380, doi:10.1002/2015JD023334, 2016.

Austin, J., K. Tourpali, E. Rozanov, H. Akiyoshi, S. Bekki, G. Bodeker, C. Brühl, N. Butchart, M. Chipperfield,
565    M. Deushi, V. I. Fomichev, M. A. Giorgetta, L. Gray, K. Kodera, F. Lott, E. Manzini, D. Marsh, K. Matthes, T. Nagashima, K. Shibata, R. S. Stolarski, H. Struthers, and W. Tian. Coupled chemistry climate model simulations of the solar cycle in ozone and temperature. *J. Geophys. Res.*, 113:D11306, 2008.

Ball, W. T., J. D. Haigh, E. V. Rozanov, A. Kuchar, T. Sukhodolov, F. Tummon, A. V. Shapiro and W. Schmutz. High solar cycle spectral variations inconsistent with stratospheric ozone observations. *Nature Geoscience*,
570    9:206-209, 2016.

Bodeker, G. E., B. Hassler, P. J. Young, and R. W. Portmann. A vertically resolved, global, gap-free ozone database for assessing or constraining global climate model simulations. *Earth Syst. Sci. Data*, 5:31–43, 2013.

Brasseur, G., and P. C. Simon. Stratospheric chemical and thermal response to long-term variability in solar
575    UV irradiance. *J. Geophys. Res.*, 86:7343–7362, doi:10.1029/JC086iC08p07343, 1981.

Chiodo, G., D. R. Marsh, R. Garcia-Herrera, N. Calvo, and J. A. Garcia. On the detection of the solar signal in the tropical stratosphere. *Atmos. Chem. Phys.*, 14:5251-5269, 2014.

Cionni, I., V. Eyring, J-F. Lamarque, W. J. Randel, D. S. Stevenson, F. Wu, Bodeker, G. E., T. G. Shepherd, D. T. Shindell, and D. W. Waugh. Ozone database in support of CMIP5 simulations: Results and corresponding
580    radiative forcing. *Atmos. Chem. Phys.*, 11:11,267–11,292, 2011.

Damadeo, R. P., J. M. Zawodny, L. W. Thomason, and N. Iyer. SAGE version 7.0 algorithm: application to SAGE II. *Atmos. Meas. Tech.*, 6:3539–3561, 2013.

Deushi, M. and Shibata, K. Development of a Meteorological Research Institute chemistry-climate model version 2 for the study of tropospheric and stratospheric chemistry. *Pap. Meteorol. Geophys.*, 62:1-46, 2011.

585    Dhomse, S., M. P. Chipperfield, R. P. Damadeo, J. M. Zawodny, W. T. Ball, W. Feng, R. Hossaini, G. W. Mann, and J. D. Haigh. On the ambiguous nature of the 11 year solar cycle signal in upper stratospheric ozone. *Geophys. Res. Lett.*, 43:7241–7249, 2016.

Dufresne, J.-L., Foujols, M. A., Denvil, S., Caubel, A., Marti, O., Aumont, O., Balkanski, Y., Bekki, S., Bellenger, H., Benshila, R., Bony, S., Bopp, L., Braconnot, P., Brockmann, P., Cadule, P., Cheruy, F., Codron, F.,
590    Cozic, A., Cugnet, D., de Noblet, N., Duvel, J.-P., Ethé, C., Fairhead, L., Fichefet, T., Flavoni, S., Friedlingstein, P., Grandpeix, J.-Y., Guez, L., Guilyardi, E., Hauglustaine, D., Hourdin, F., Idelkadi, A., Ghattas, J., Joussaume, S., Kageyama, M., Krinner, G., Labetoulle, S., Lahellec, A., Lefebvre, M.-P., Lefevre, F., Levy, C., Li, Z. X., Lloyd, J., Lott, F., Madec, G., Mancip, M., Marchand, M., Masson, S., Meurdesoif, Y., Mignot, J., Musat, I., Parouty, S., Polcher, J., Rio, C., Schulz, M., Swingedouw, D., Szopa, S., Talandier, C., Terray,
595    P., Viovy, N., and Vuichard, N. Climate change projections using the IPSL-CM5 Earth System Model: from CMIP3 to CMIP5. *Clim. Dyn.*, 40:2123–2165, 2013.

Ermolli, I., K. Matthes, T. Dudok de Wit, N. A. Krivova, K. Tourpali, M. Weber, Y. C. Unruh, L. Gray, U. Langematz, P. Pilewskie, E. Rozanov, W. Schmutz, A. Shapiro, S. K. Solanki, G. Thuillier, and T. N. Woods. Re-

cent variability of the solar spectral irradiance and its impact on climate modelling. *Atmos. Chem. Phys.*, 13:
600   3945–3977, 2013.

Eyring, V., J. M. Arblaster, I. Cionni, J. Sedláček, J. Perlwitz, P. J. Young, S. Bekki, D. Bergmann, P. Cameron-
Smith, W. J. Collins, G. Faluvegi, K.-D. Gottschaldt, L. W. Horowitz, D. E. Kinnison, J.-F. Lamarque, D. R.
Marsh, D. Saint-Martin, D. T. Shindell, K. Sudo, S. Szopa, and S. Watanabe. Long-term ozone changes and
associated climate impacts in CMIP5 simulation. *J. Geophys. Res.*, 118:5029–5060, 2013.

605   Frith, S. M., N. A. Kramarova, R. S. Stolarski, R. D. McPeters, P. K. Bhartia and G. J. Labow. Recent changes
in column ozone based on the SBUV version 8.6 merged ozone database. *J. Geophys. Res.*, 119:9735–9751,
2014.

Forster, P. M., V. I. Fomichev, E. Rozanov, C. Cagnazzo, A. I. Jonsson, U. Langematz, B. Fomin, M. J. Iacono,
B. Mayer, E. Mlawer, G. Myhre, R. W. Portmann, H. Akiyoshi, V. Falaleeva, N. Gillett, A. Karpechko, J. Li,
610   P. Lemennais, O. Morgenstern, S. Oberländer, M. Sigmond, and K. Shibata. Evaluation of radiation scheme
performance within chemistry-climate models. *J. Geophys. Res.*, 116:D10302, 2011.

Giorgetta, M. A., J. Jungclaus, C. H. Reick, S. Legutke, J. Bader, M. Böttinger, V. Brovkin, T. Crueger, M.
Esch, K. Fieg, K. Glushak, V. Gayler, H. Haak, H.-D. Hollweg, T. Ilyina, S. Kinne, L. Kornblueh, D. Matei,
T. Mauritsen, U. Mikolajewicz, W. Mueller, D. Notz, F. Pithan, T. Raddatz, S. Rast, R. Redler, E. Roeckner,
615   H. Schmidt, R. Schnur, J. Segschneider, K. D. Six, M. Stockhause, C. Timmreck, J. Wegner, H. Widmann,
K.-H. Wieners, M. Claussen, J. Marotzke, B. Stevens. Climate and carbon cycle changes from 1850 to 2100
in MPI-ESM simulations for the Coupled Model Intercomparison Project phase 5. *Journal of Advances in
Modeling Earth Systems*, 5:572-597, 2013.

Gray, L. J., S. Rumbold, and K. P. Shine. Stratospheric temperatures and radiative forcing response to 11-year
620   solar cycle changes in irradiance and ozone. *J. Atmos. Sci.*, 66:2402–2417, 2009.

Gray, L. J., J. Beer, M. Geller, J. D. Haigh, M. Lockwood, K. Matthes, U. Cubasch, D. Fleitmann, G. Harrison,
L. Hood, J. Luterbacher, G. A. Meehl, D. Shindell, B. van Geel, and W. White. Solar influences on climate.
*Rev. Geophys.*, 48:RG4001, 2010.

Haigh, J. D. The role of stratospheric ozone in modulating the solar radiative forcing of climate. *Nature*, 370:
625   544–546, 1994.

Haigh., J. D., A. R. Winning, R. Toumi, and J. W. Harder. An influence of solar spectral variations on radiative
forcing of climate. *Nature*, 467:696–699, 2010.

Harris, N. R. P., B. Hassler, F. Tummon, G. E. Bodeker, D. Hubert, I. Petropavlovsikh, W. Steinbrecht, J.
Anderson, P. K. Bhartia, C. D. Boone, A. Bourassa, S. M. Davis, D. Degenstein, A. Delcloo, S. M. Frith, L.
630   Froidevaux, S. Godin-Beekmann, N. Jones, M. J. Kurylo, E. Kyrölä, M. Laine, S.T. Leblanc, J.C. Lambert,
E. Mahieu, A. C. Maycock, M. de Maziere, A. Parrish, R. Querel, K. H. Rosenlof, C. Roth, C. Sioris, B.
Liley, J. Staehelin, R. S. Stolarski, R. Stubi, J. Tamminen, C. Vigouroux, K. Walker, H. J. Wang, J. Wild, and
J. M. Zawodny. Past changes in the Vertical Distribution of Ozone, Part III: Analysis and Interpretation of
Trends. *Atmos. Chem. Phys. Diss.*, 15:8565–8608, 2015.

635   Hassler, B., G. E. Bodeker, M. Dameris. Technical Note: A new global database of trace gases and aerosols
from multiple sources of high vertical resolution measurements. *Atmos. Chem. Phys.*, 8:5403–5421, 2008.

Hood, L. L., S. Misios, D. M. Mitchell, E. Rozanov, L. J. Gray, K. Tourpali, K. Matthes, H. Schmidt, G. Chiodo, R. Thiéblemont, D. Shindell, and A. Krivolutsky. Solar signals in CMIP-5 simulations: The ozone response. *Q. J. Roy. Meteorol. Soc.*, 141, 2670–2689, 2015. doi:10.1002/qj.2553.

640 Iacono, M. J., J. S. Delamere, E. J. Mlawer, M. W. Shephard, S. A. Clough, and W. D Collins. Radiative forcing by long-lived greenhouse gases: Calculations with the AER radiative transfer models. *Journal of Geophysical Research: Atmospheres*, 113:D13103, 2008.

Imai, K., Manago, N., Mitsuda, C., Naito, Y., Nishimoto, E., Sakazaki, T., Fujiwara, M., Froidevaux, L., von Clarmann, T., Stiller, G. P., Murtagh, D. P., Rong, P.-P., Mlynczak, M. G., Walker, K. A., Kinnison, D. E., 645 Akiyoshi, H., Nakamura, T., Miyasaka, T., Nishibori, T., Mizobuchi, S., Kikuchi, K., Ozeki, H., Takahashi, C., Hayashi, H., Sano, T., Suzuki, M., Takayanagi, M., and Shiotani, M. Validation of ozone data from the Superconducting Submillimeter-Wave Limb-Emission Sounder (SMILES). *J. Geophys. Res. Atmos.*, 118: 5750–5769, doi:10.1002/jgrd.50434, 2013.

Jöckel, P., H. Tost, A. Pozzer, M. Kunze, O. Kirner, C. A. M. Brenninkmeijer, S. Brinkop, D. S. Cai, C. Dyroff, 650 J. Eckstein, F. Frank, H. Garny, K.-D. Gottschaldt, P. Graf, V.Grewe, A. Kerkweg, B. Kern, S. Matthes, M. Mertens, S. Meul, M. Neumaier, M. Nützel, S. Oberländer-Hayn, R. Ruhnke, T. Runde, R. Sander, D. Scharffe, and A. Zahn. Earth System Chemistry integrated Modelling (ESCiMo) with the Modular Earth Submodel System (MESSy) version 2.51. *Geosci. Model Dev.*, 9:1153-1200, doi:10.5194/gmd-9-1153-2016, 2016.

655 Jonsson, A. I., J. de Grandpré, V. I. Fomichev, J. C. McConnell and S. R. Beagley Doubled CO2-induced cooling in the middle atmosphere: Photochemical analysis of the ozone radiative feedback. *J. Geophys. Res*, 109:D24103, doi:10.1029/2004JD005093, 2004.

Kyrölä, E., M. Laine, V. Sofieva, J. Tamminen, S. M. Päivärinta, S. Tukiainen, J. Zawodny and L. Thomason. Combined SAGE II-GOMOS ozone profile data set for 1984–2011 and trend analysis of the vertical 660 distribution of ozone. *Atmos. Chem. Phys.*, 13:10645–10658, 2013.

Kuroda, Y. and K. Kodera. Effect of solar activity on the Polar-night Jet Oscillation in the Northern and Southern hemisphere winter. *J. Met. Soc. Japan*, 80:973–984, 2002.

Marchand M., Keckhut, P., Lefebvre, S., Claud, C., Cugnet, D., Hauchecorne, A., Lefèvre, F., Jumelet, J., Lott, F., Hourdin, F., Thuillier, G., Poulain, V., Bossay, S., Lemennais, P., David, C., and Bekki, S. Dynami-665 cal amplification of the stratospheric solar response simulated with the chemistry-climate model LMDz-REPROBUS. *J. Atmos. Sol. Terr. Phy.*, 75-76:147–160, 2012.

Marsh, D. R. M., D. E. Mills, J. F. Kinnison, N. C. Lamarque, and L. M. Polvani Climate change from 1850 to 2005 simulated in CESM1(WACCM). *J. Clim.*, 26, 7372-7391, doi:10.1175/JCLI-D-12-00558.1, 2013.

Matthes, K., Y. Kuroda, K. Kodera, and U. Langematz. Transfer of the solar signal from the stratosphere to the 670 troposphere: Northern winter. *J. Geophys. Res.*, 111:D06108, 2006.

Matthes, K. et al. Solar forcing recommendation for CMIP6. *Geosci. Mod. Devel. Discuss.*, submitted, 2017.

Maycock, A. C., S. Ineson, L. J. Gray, A. Scaife, J. Anstey, M. Lockwood, N. Butchart, S. Hardiman, D. Mitchell, S. Osprey. Possible impacts of a future grand solar minimum on climate: Stratospheric and global circulation changes *J. Geophys. Res.*, doi:10.1002/2014JD022022, 2015.

675  Maycock, A. C., K. Matthes, S. Tegtmeier, R. Thiéblemont, L. L. Hood. The representation of solar cycles
      signals in stratospheric ozone. Part I: A comparison of satellite observations *Atmos. Chem. Phys. Diss.*,
      doi:10.5194/acp-2015-882, 2016.

Michou, M., Saint-Martin, D., Teyssèdre, H., Alias, A., Karcher, F., Olivié, D., Voldoire, A., Josse, B., Peuch,
      V.-H., Clark, H., Lee, J. N., and Chéroux, F. A new version of the CNRM Chemistry-Climate Model, CNRM-
680   CCM: description and improvements from the CCMVal-2 simulations. *Geosci. Model Dev.*, 4:873–900,
      doi:10.5194/gmd-4-873-2011, 2011.

Mitchell, D. M., L. J. Gray, M. Fujiwara, T. Hibino, J. Anstey, Y. Harada, C. Long, S. Misios, P. A. Stott, and
      D. Tan. Signatures of natural variability in the atmosphere using multiple reanalysis datasets. *Q. J. Roy.
      Meteorol. Soc.*, in press, 2015a. doi:10.1002/qj.2492.

685  Mitchell, D. M., S. Misios, L. J. Gray, K. Tourpali, K. Matthes, L. L. Hood, H. Schmidt, G. Chiodo, R. Thiéble-
      mont, E. Rozanov, D. Shindell, and A. Krivolutsky. Solar signals in CMIP-5 simulations: the stratospheric
      pathway. *Q. J. Roy. Meteorol. Soc.*, in press, 2015b. doi:10.1002/qj.2530.

Misios, S., D. M. Mitchell, L. J. Gray, K. Tourpali, K. Matthes, L. L. Hood, H. Schmidt, G. Chiodo, R. Thiéble-
      mont, E. Rozanov, and A. Krivolutsky. Solar signals in CMIP-5 simulations: effects of atmosphere–ocean
690   coupling. *Q. J. Roy. Meteorol. Soc.*, 142: 928–941, 2016. doi:10.1002/qj.2695.

Morgenstern, O., M. I. Hegglin, E. Rozanov, F. M. O'Connor, N. L. Abraham, H. Akiyoshi, A. T. Archibald,
      S. Bekki, N. Butchart, M. P. Chipperfield, M. Deushi, S. S. Dhomse, R. R. Garcia, S. C. Hardiman, L. W.
      Horowitz, P. Jöckel, B. Josse, D. Kinnison, M. Lin, E. Mancini, M. E. Manyin, M. Marchand, V. Marécal,
      M. Michou, L. D. Oman, G. Pitari, D. A. Plummer, L. E. Revell, D. Saint-Martin, R. Schofield, A. Stenke,
695   K. Stone, K. Sudo, T. Y. Tanaka, S. Tilmes, Y. Yamashita, K. Yoshida, and G. Zeng. Review of the global
      models used within phase 1 of the Chemistry-Climate Model Initiative (CCMI) *Geosci. Model Dev.*, 10,
      639-671, doi:10.5194/gmd-10-639-2017, 2017.

Nissen, K. M., K. Matthes, U. Langematz, and B. Mayer. Towards a better representation of the solar cycle in
      general circulation models. *Atmos. Chem. Phys.*, 7:5391–5400, 2007.

700  Osprey, S. M., L. J. Gray, Steven C. Hardiman, N. Butchart, and T. J. Hinton. Stratospheric variability in the
      20th century CMIP5 simulations of the Met Office climate model: High-top versus low-top. *J. Clim.*, 26:
      1595–1606, 2013.

Penner, J. E., and Chang, J. S. Possible variations in atmospheric ozone related to the eleven-year solar cycle
      *Geophys. Res. Lett.*, 5:817–820, doi:10.1029/GL005i010p00817, 1978.

705  Pincus, R. and B. Stevens. Paths to accuracy for radiation parameterizations in atmospheric models. *J. Adv.
      Model. Earth Syst.*, 5:225-233, 2013.

Ramaswamy, V., M. L. Chanin, J. Angell, J. Barnett, D. Gaffen, M. Gelman, P. Keckhut, Y. Koshelkov, K. Lab-
      itzke, J.-J. R. Lin, A. O'Neill, J. Nash, W. Randel, R. Rood, K. Shine, M. Shiotani, R. Swinbank Stratospheric
      temperature trends: Observations and model simulations. *Rev. Geophys.*, 39:71-122, 2001.

710  Randel, W. J. and F. Wu. A stratospheric ozone profile data set for 1979–2005: Variability, trends, and compar-
      isons with column ozone data. *J. Geophys. Res.*, 112:D06313, 2007.

Rayner, N. A., D. E. Parker, E. B. Horton, C. K. Folland, L. V. Alexander, D. P. Rowell, E. C. Kent, and
      A. Kaplan. Global analyses of sea surface temperature, sea ice, and night marine air temperature since the
      late nineteenth century. *J. Geophys. Res.*, 108:4407–4435, 2003.

715    Revell, L. E., Tummon, F., Stenke, A., Sukhodolov, T., Coulon, A., Rozanov, E., Garny, H., Grewe, V., and Peter, T. Drivers of the tropospheric ozone budget throughout the 21st century under the medium-high climate scenario RCP 6.0. *Atmos. Chem. Phys.*, 15:5887–5902, doi:10.5194/acp-15-5887-2015, 2015.

Sato, M., J. E. Hansen, M. P. McCormick, and J.B. Pollack. Stratospheric aerosol optical depth, 1850-1990. *J. Geophys. Res.*, 98:22,987–22,994, 1993.

720    Schmidt, H., S. Rast, F. Bunzel, M. Esch, M. Giorgetta, S. Kinne, T. Krismer, G. Stenchikov, C. Timmreck, L. Tomassini, and M. Walz. Response of the middle atmosphere to anthropogenic and natural forcings in the CMIP5 simulations with the Max Planck Institute Earth system model. *J. Adv. Model. Earth Syst.*, 5:98–116, 2013.

Scinocca, J. F., N. A. McFarlane, M. Lazare, J. Li and D. Plummer. Technical Note: The CCCma third
725    generation AGCM and its extension into the middle atmosphere. *Atmos. Chem. Phys.*, 8:8, 7055–7074, doi:10.5194/acp-8-7055-2008, 2008.

Shibata, K. and K. Kodera. Simulation of radiative and dynamical responses of the middle atmosphere to the 11-year solar cycle. *J. Atmos. Sol. Terr. Phys.*, 67:125–143, 2005.

Solomon, S., D. Kinnison, J. Bandoro, and R. Garcia Simulation of polar ozone depletion: An update. *J.*
730    *Geophys. Res. Atmos.*, 120:7958–7974, doi:10.1002/2015JD023365, 2015.

Soukharev, B. E. and L. L. Hood. Solar cycle variation of stratospheric ozone: Multiple regression analysis of long-term satellite data sets and comparisons with models. *J. Geophys. Res.*, 111:D20314, 2006.

Sukhodolov, T., Rozanov, E., Shapiro, A. I., Anet, J., Cagnazzo, C., Peter, T., and Schmutz, W. Evaluation of the ECHAM family radiation codes performance in the representation of the solar signal. *Geosci. Model*
735    *Dev.*, 7:2859-2866, doi:10.5194/gmd-7-2859-2014, 2014.

Sukhodolov, T., E. Rozanov, W. T. Ball, A. Bais, K. Tourpali, A. I. Shapiro, P. Telford, S. Smyshlyaev, B. Fomin, R. Sander, S. Bossay, S. Bekki, M. Marchand, M. P. Chipperfield, S. Dhomse, J. D. Haigh, T. Peter, W. Schmutz Evaluation of simulated photolysis rates and their response to solar irradiance variability. *J. Geophys. Res.*, 121:6066–6084, doi:10.1002/2015JD024277, 2016.

740    SPARC CCMVal. SPARC report on the evaluation of Chemistry-Climate Models [V. Eyring, T. G. Shepherd and D. Waugh (Eds.)], SPARC Report No. 5, WCRP-132,WMO/TD-No. 1526, 2010.

Stenke, A., Schraner, M., Rozanov, E., Egorova, T., Luo, B., and Peter, T. The SOCOL version 3.0 chemistry-climate model: description, evaluation, and implications from an advanced transport algorithm. *Geosci. Model Dev.*, 6:1407–1427, doi:10.5194/gmd-6-1407-2013, 2013.

745    Stevens, B., M. Giorgetta, M. Esch, T. Mauritsen, T. Crueger, S. Rast, M. Salzmann, H. Schmidt, J. Bader, K. Block, R. Brokopf, I. Fast, S. Kinne, L. Kornblueh, U. Lohmann, R. Pincus, T. Reichler, E. Roeckner. Atmospheric component of the MPI M Earth System Model: ECHAM6. Journal of Advances in Modeling Earth Systems. *Journal of Advances in Modeling Earth Systems*, 5:146-172, 2013.

Szopa, S., Balkanski, Y., Schulz, M., Bekki, S., Cugnet, D., Fortems-Cheiney, A., Turquety, S., Cozic, A.,
750    Déandreis, C., Hauglus- taine, D., Idelkadi, A., Lathière, J., Lefèvre, F., Marchand, M., Vuolo, R., Yan, N., and Dufresne, J.-L. Aerosol and ozone changes as forcing for climate evolution between 1850 and 2100. *Clim. Dyn.*, 40:2223–2250, 2013.

Tummon, F., B. Hassler, N. R. P. Harris, J. Staehelin, W. Steinbrecht, J. Anderson, G. E. Bodeker, A. Bourassa, S. M. Davis, D. Degenstein, S. M. Frith, L. Froidevaux, E. Kyrölä, M. Laine, C. Long, A. A. Penckwitt, C. E.

755    Sioris, K. H. Rosenlof, C. Roth, H. J. Wang, and J. Wild. Intercomparison of vertically resolved merged
       satellite ozone data sets: interannual variability and long-term trends. *Atmos. Chem. Phys.*, 15:3021-3043,
       2015.

       Voldoire A., Sanchez-Gomez, E., Salas y Mélia, D., Decharme, B., Cassou, C., Sénési, S., Valcke, S., Beau,
       I., Alias, A., Chevallier, M., Déqué, M., Deshayes, J., Douville, H., Fernandez, E., Madec, G., Maisonnave,
760    E., Moine, M.-P., Planton, S., Saint-Martin, D., Szopa, S., Tytéca, S., Alkama, R., Bélamari, S., Braun, A.,
       Coquart, L., and Chauvin, F. The CNRM-CM5.1 global climate model: description and basic evaluation.
       *Clim. Dyn.*, 40:2091–2121, doi:10.1007/s00382-011-1259-y, 2012.

       Wang, Y.-M., J. L. Lean, and N. R. Shelley. Modeling the Sun's magnetic field and irradiance since 1713. *J.
       Astrophys.*, 625:522–538, 2005.

765    Yukimoto, S., Yoshimura, H., Hosaka, M., Sakami, T., Tsujino, H., Hirabara, M., Tanaka, T. Y., Deushi, M.,
       Obata, A., Nakano, H., Adachi, Y., Shindo, E., Yabu, S., Ose, T., and Kitoh, A. Meteorological Research
       Institute Earth System Model Version 1 (MRI-ESM1) – Model Description. *Tech. Rep. of MRI*, 64:83pp.,
       2011.

       Yukimoto, S., Adachi, Y., Hosaka, M., Sakami, T., Yoshimura, H., Hirabara, M., Tanaka, T. Y., Shindo, E.,
770    Tsujino, H., Deushi, M., Mizuta, R., Yabu, S., Obata, A., Nakano, H., Koshiro, T., Ose, T., and Kitoh, A. A
       new global climate model of the Meteorological Research Institute: MRI-CGCM3 – Model description and
       basic performance. *J. Meteorol. Soc. Jpn.*, 90:23-64, 2012.

| Model | QBO | No. shortwave bands | Reference |
|---|---|---|---|
| CMAM | No | 4 | Jonsson et al. (2004); Scinocca et al. (2008) |
| CESM1(WACCM) | Nudged | 19 | Marsh et al. (2013); Solomon et al. (2015) |
| CCSRNIES-MIROC3.2 | Nudged | 20 | Imai et al. (2011); Akiyoshi et al. (2016) |
| CNRM-CM5-3 | No | 6 | Voldoire et al. (2011); Michou et al. (2015); http://www.cnrm-game-meteo.fr/ |
| EMAC(L90) | Nudged | 55 in the stratosphere (<70 hPa) | Jöckel et al. (2016) |
| LMDz-REPROBUS-CM5 (L39) | No | 2 | Marchand et al. (2011); Szopa et al. (2013); Dufresne et al. (2013) |
| MRI-ESM1r1 | Internal | 22 | Yukimoto et al. (2011, 2012); Deushi and Shibata (2011) |
| SOCOL3 | Nudged | 6 | Stenke et al. (2013); Revell et al. (2015) |

**Table 1.** Details of the CCMI-1 models used in this study. See Morgenstern et al. (2017) for more details.
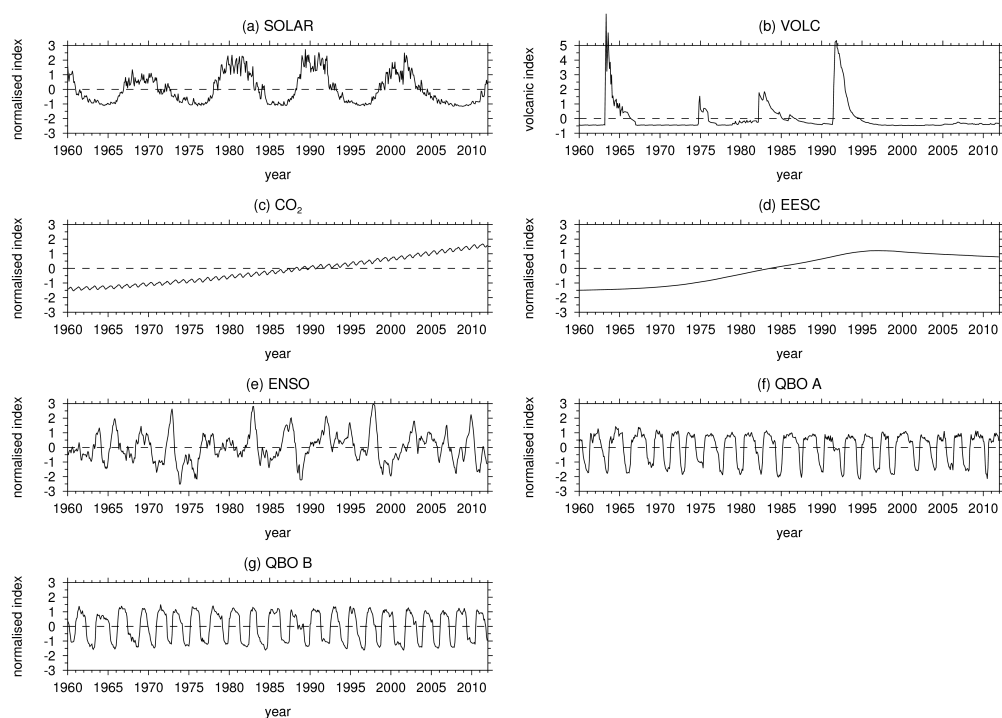
**Figure 1.** Timeseries of the seven basis functions used in the MLR analysis. (a) Solar forcing based on F10.7cm flux; (b) volcanic forcing based on the Sato AOD index; (c) $CO_2$; (d) equivalent effective stratospheric chlorine; (e) ENSO index; (f, g) two orthogonal QBO indices defined as the first two principal component timeseries of tropical zonal mean zonal winds. The timeseries are in units of standard deviation.
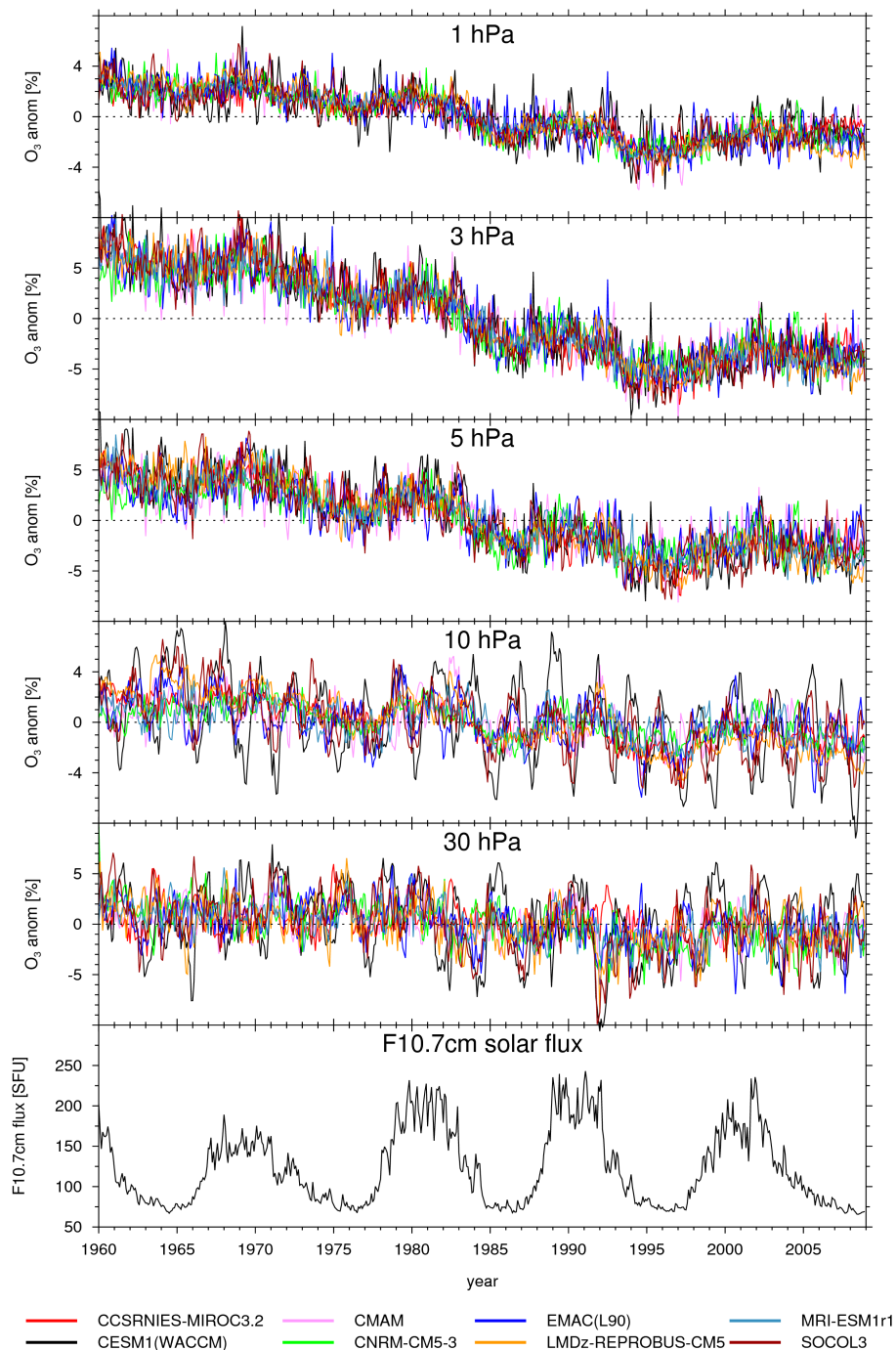
**Figure 2.** Timeseries of deseasonalised percent tropical (30°S-30°N) ozone anomalies in CCMI-1 models for 1960-2009 at 1 hPa, 3 hPa, 5 hPa, 10 hPa and 30 hPa. The lowest panel shows the F10.7 cm solar flux for reference.
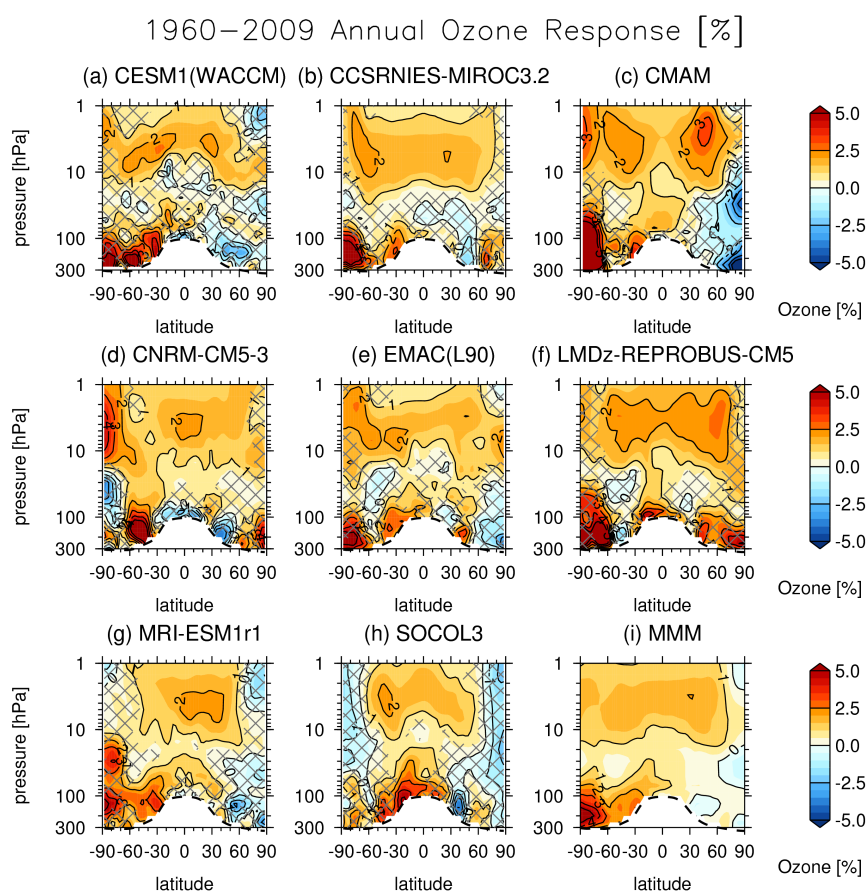
**Figure 3.** The percent (%) differences in stratospheric ozone mixing ratios per 130 SFU for 1960-2009 in the CCMI-1 models listed in Table 1. The solid contours denote 1% intervals. Hatching denotes regions where the regression coefficients are not significantly different from zero at the 95% confidence level. Panel (i) shows the multi-model mean (MMM). Tropospheric values have been masked out.
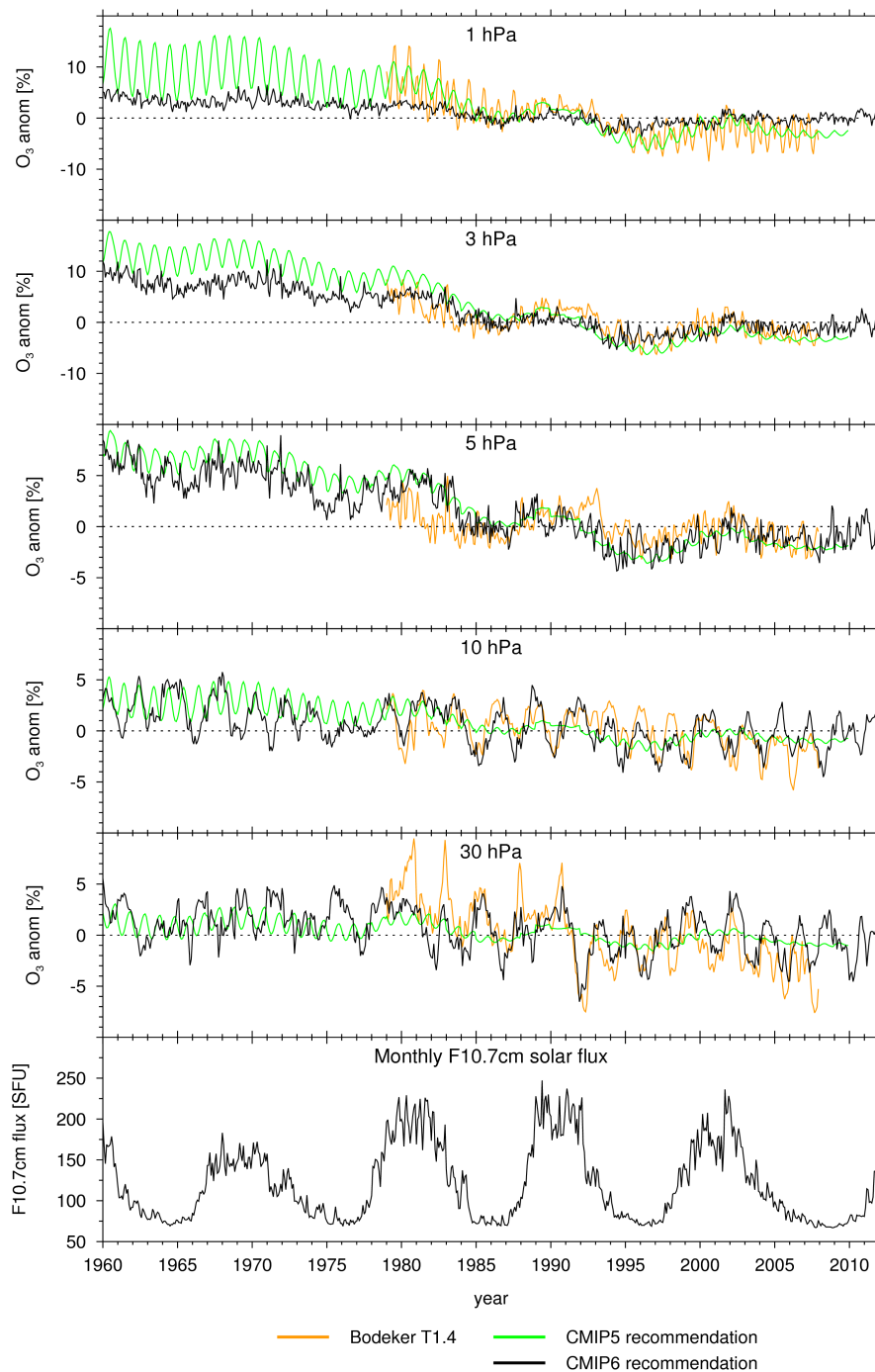
**Figure 4.** Timeseries of deseasonalised percent tropical (30°S-30°N) ozone anomalies from the Bodeker, CMIP5 (Cionni et al., 2011), and CMIP6 ozone databases for 1960-2011 at (a) 1 hPa, (b) 3 hPa, (c) 5 hPa, (d) 10 hPa and (e) 30 hPa. The lowest panel shows the F10.7 cm solar flux for reference.
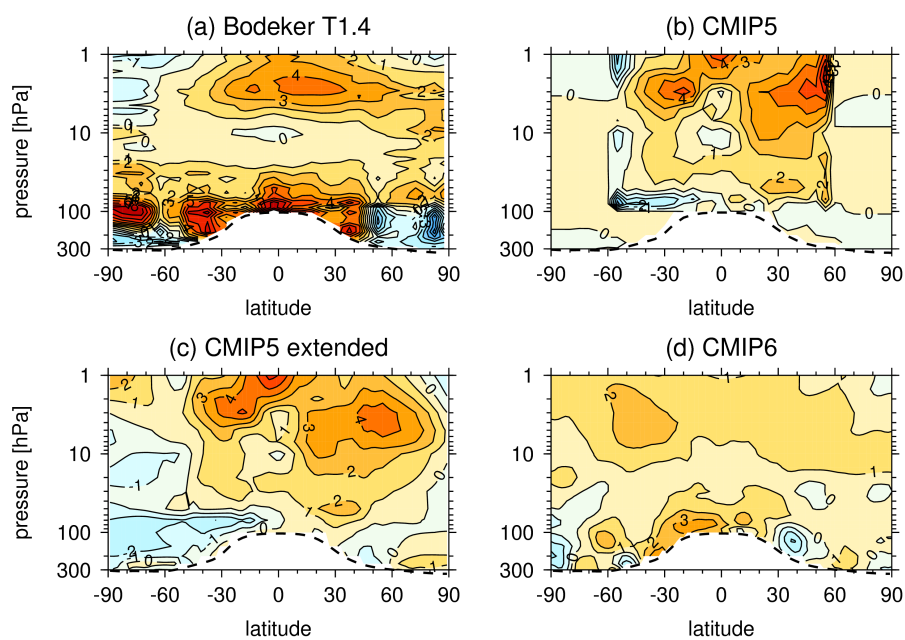
**Figure 5.** The annual mean percent (%) differences in ozone per 130 SFU over 1979-2007 for the (a) Bodeker,

(b) CMIP5, (c) Extended CMIP5 and (d) CMIP6 ozone databases. The contour interval is 1%.
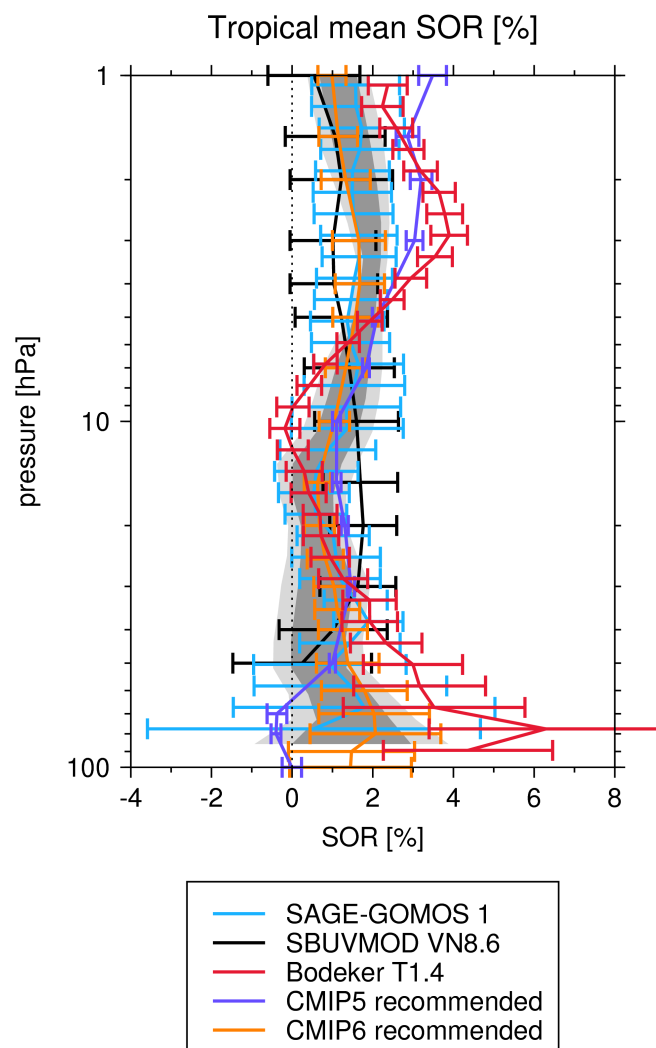
**Figure 6.** Vertical profiles of the tropical (30°S-30°N) average annual SOR per 130 SFU (%). The range of the best estimates across the eight CCMI-1 models is shown in the dark grey shading. The light grey shading shows ±1 standard deviation of the intermodel spread in SOR across the CCMI-1 models. The coloured lines show the tropical mean annual SOR in the three climate model ozone databases discussed in Section 3.2 and two satellite ozone datasets from Maycock et al. (2016) (SBUVMOD VN8.6 and SAGE-GOMOS 1). The whiskers denote 2.5-97.5% confidence intervals.
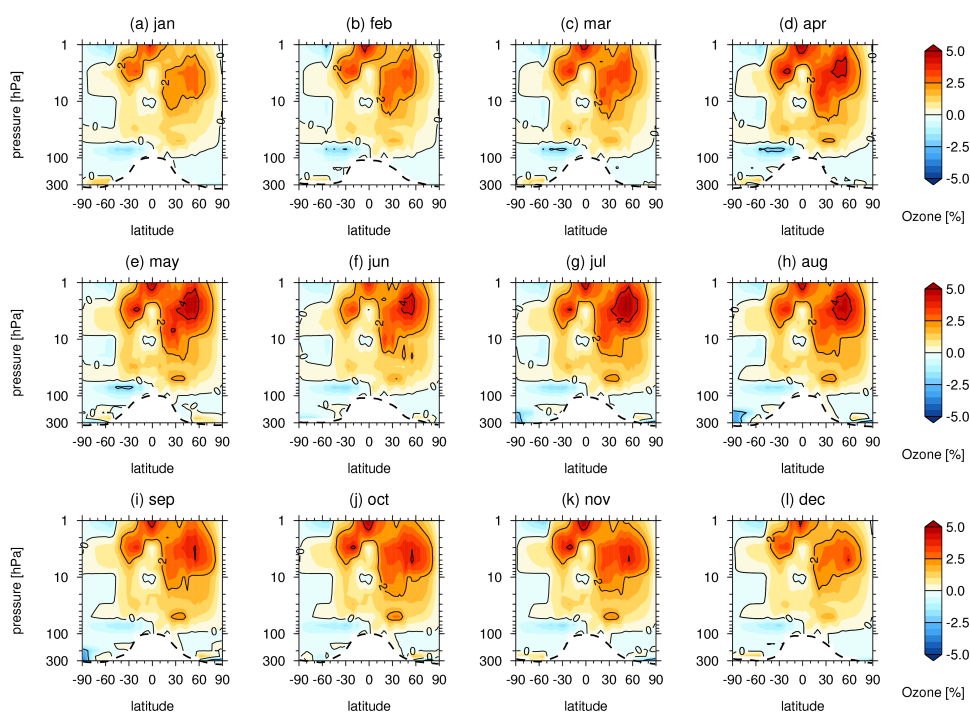
**Figure 7.** Monthly mean percent (%) ozone anomalies per 130 SFU for (a) January to (l) December in the Extended CMIP5 ozone database. The solid contours denote 2% intervals.
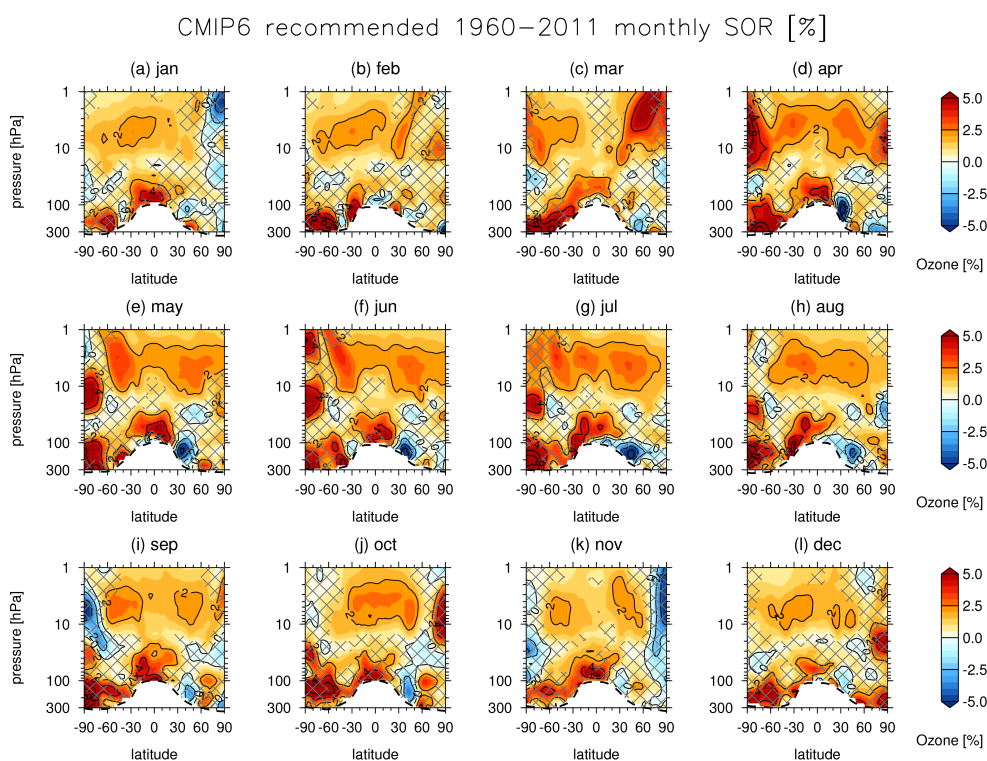
**Figure 8.** Monthly mean percent (%) ozone anomalies per 130 SFU for (a) January to (l) December in the CMIP6 ozone database. The solid contours denote 2% intervals. Hatching denotes regions where the regression coefficients are not significantly different from zero at the 95% confidence level.
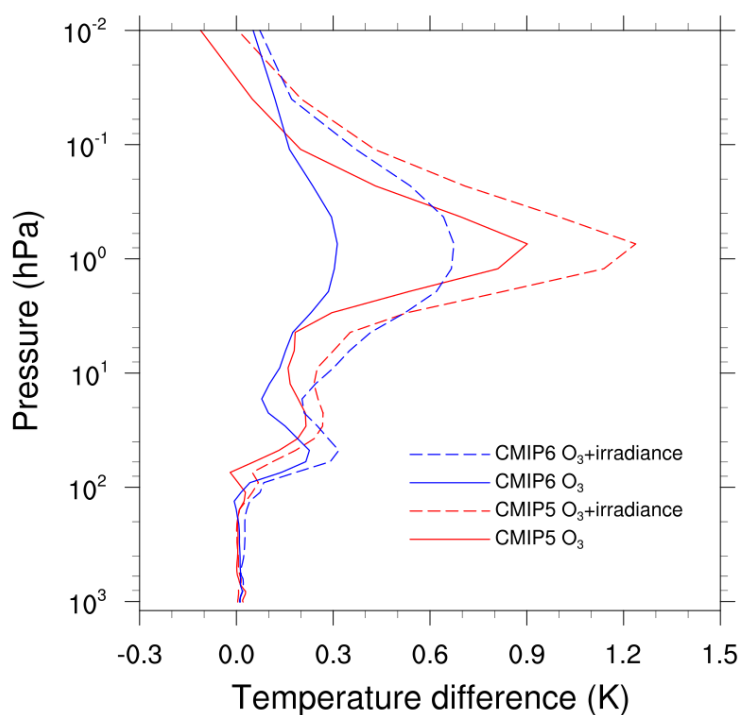
**Figure 9.** Average tropical (30°S-30°N) solar cycle (max-min) temperature anomalies as simulated by ECHAM6. Anomalies have been calculated between four sensitivity experiments representing different solar maximum conditions and a reference experiment representing solar minimum conditions. The sensitivity experiments are performed by prescribing: (red solid) SOR from the Extended CMIP5 ozone database; (red dashed) recommended SOR and spectral solar irradiance anomalies for CMIP5; (blue solid) historical SOR from recommended CMIP6 ozone database; and (blue dashed) recommended SOR and spectral solar irradiance anomalies for CMIP6.